Use of Polyaniline Coating on Magnetic MoO_3 and its Effects on Material Stability and Visible-Light Photocatalysis of Tetracycline

Sofia K. Fanourakis[1], Sharona Q. Barroga[2,3], Riya A. Mathew[4], Janire Peña-Bahamonde[4], Stacey M. Louie[4], Jem Valerie D. Perez[2], Debora F. Rodrigues[1,4]*

[1] Department of Materials Science and Engineering, University of Houston, Houston, TX 77204 – 4003

[2] Department of Chemical Engineering, University of the Philippines,

[3] Department of Chemical Engineering, Mariano Marcos State University,

[4] Department of Civil and Environmental Engineering, University of Houston, Houston, TX 77204 – 4003

* Corresponding Author: Debora F. Rodrigues, email: dfrigirodrigues@uh.edu

Abstract

A semiconducting material (polyaniline-coated magnetic MoO_3) with photodegradative properties and low solubility was synthesized and assessed in the degradation of tetracycline to address the rising concern of antibiotics in water systems. Polyaniline (PANI) provided a protective coating, significantly reducing MoO_3 dissolution across a wide pH range, while the Fe_3O_4 core facilitated photocatalyst extraction from water. Uncoated MoO_3@Fe_3O_4 dissolution significantly increased with increasing pH (dissolved 2.9% at pH 3 and 22.9% at pH 10). With the PANI coating, dissolution was reduced to 1.6% at pH 3 and 5.6% at pH 10. TC removal by PANI@MoO_3@Fe_3O_4 was 8.2 mg TC/g photocatalyst in visible light and 6.5 mg/g in dark within 35 minutes under optimum conditions. PANI@MoO_3@Fe_3O_4 tetracycline degradative properties were facilitated by reactive species produced from water oxidation by photogenerated h^+. Our initial assessment of PANI@MoO_3@Fe_3O_4 as a photocatalyst for pharmaceutical contaminant degradation indicates PANI@MoO_3@Fe_3O_4 is a promising material useful for wider environmental applications.

Keywords: nanoparticles, photocatalysis, tetracycline, antibiotics, polymer coatings.

1. Introduction

As pharmaceutical production and use continue to increase, contamination of waterways due to emerging pharmaceutical contaminants (EPCs) has been of rising concern. Many EPCs in the environment have shown to bioaccumulate and persist in soils, plant tissues, and aquatic environments leading to acute and long term harm [1,2]. Conventional methods of removing EPCs such as filtration, adsorption-based, and advanced oxidation processes can have significant drawbacks. For instance, filtration and adsorption-based processes present low removal of several EPCs (sulfamethoxazole, venlafaxine, piroxicam, among others) and produce sludge containing the removed EPCs, which is a major source of secondary pollution [1,2]. Advanced oxidation processes (such as ozonation and UV radiation) are able to break down pollutants, however, they are energy intensive and costly, and most are unable to fully degrade pharmaceutical contaminants [1,2]. As such, there has been considerable research interest in investigating visible light photocatalytic materials, in particular metal oxides, which are less energy intensive and have demonstrated their effectiveness in degrading a variety of EPCs (analgesics, antibiotics, and anticoagulants, among others) [1–10]. MoO_3, a promising visible light photocatalyst, is easily synthesized and modified in terms of size and morphology and has demonstrated its utility in energy storage, field-effect transistors, thermoelectric devices, gas sensing, among others [11]. Furthermore, MoO_3 is vastly underutilized in the degradation of EPCs [1,2]. Only recently, MoO_3-based materials have begun to be studied for pharmaceutical contamination removal and have demonstrated effective removal of a variety of EPCs: ibuprofen [7], diclofenac [6], tetracycline [12–15], ofloxacin [16], trimethoprim [3], metronidazole [17,18], and ciprofloxacin [19]. However, an important drawback of MoO_3-based materials used in water treatment is their high solubility, which can greatly reduce their long term effectiveness and introduce additional water contamination, thus, reducing their usability in water treatment [11,20,21]. Despite this limitation, to our knowledge, no study has investigated a mechanism to reduce the solubility of MoO_3 in aquatic systems in conjunction with examining whether MoO_3 photocatalytic activity can be maintained in the degradation of EPCs.

To reduce the solubility of metal oxides, polymer coatings, and in particular, conductive coatings, can be utilized [22–27]. The conductivity of such coatings has been shown to contribute towards enhanced material stability against structural collapse or dissolution [22–27] and enhanced photocatalytic activity [25,27–33]. Polyaniline (PANI) is one such conductive polymer, which has notable advantages over other conductive polymers, namely, environmental stability, high conductivity, good electrochemical activity, ease and low cost of synthesis, and biocompatibility [34–36]. These properties have made it particularly appealing for use in water treatment. For instance, the incorporation of PANI on TiO_2-based materials has led to improved ability of the nanocomposite to photodegrade methylene blue [32] and azo dye, while remaining stable even after solar irradiation [33]. PANI was further demonstrated to improve photodegradative properties in the degradation of dyes when coated on MoO_3 [37] or ZnO [38], and in the degradation of tetraethylated rhodamine when coated on Bi_2WO_3 [25]. These improvements were attributed to the increase of photogenerated electron-hole pair separation and decrease of the recombination rate [25,33]. Furthermore, PANI has shown to reduce metal oxide breakdown in solution increasing material stability, which has made it particularly useful for metal corrosion protection in basic and acidic media [24]. Additionally, PANI incorporation in material used in energy storage has demonstrated improvement of electrochemical performance, which has been partly attributed to the reduction of metal oxide structural collapse during charge-discharge cycles by providing a protective layer [26,31].

In this study, we examined the effectiveness of PANI as a coating for MoO_3 nanoparticles for application in EPC removal as well as its effectiveness in the reduction of the solubility of the underlying metal oxide material. Specifically, we studied the degradation of tetracycline (TC) by

PANI coated magnetic MoO_3 and the dissolution of the coated and uncoated material at the conditions that show the highest photocatalytic activity. TC was selected as the model contaminant as it is an antibiotic of particular environmental concern, negatively impacting the environment and harming human health [8]. TC is one of the most widely utilized antibiotics, especially in animal feed and, due to its poor absorption by people and animals, an alarming amount of this compound and its metabolites are released into the environment [8,39]. It has also been demonstrated that it can contribute towards emergence of bacterial antibiotic resistance in water and wastewater [1,39,40], which make the presence of such antibiotic in water systems alarming. The magnetic MoO_3 (MoO_3@Fe_3O_4) utilized in this study, has previously demonstrated photocatalytic properties in methylene blue degradation and is easily removable from water due to its magnetic properties [27,41]. The synthesized PANI@MoO_3@Fe_3O_4 (PMF) was able to improve photocatalytic activity (without yielding any detectable levels of TC degradation byproducts) as well as reduce the solubility of the uncoated material, MoO_3@Fe_3O_4 (MF). Our results demonstrate the usefulness of PANI when applied as a coating on unstable metal oxide photocatalysts in aqueous solutions, such as MoO_3 [ref]. Many metal oxide nanomaterials researched for water treatment applications are not useful in commercial settings as material dissolution greatly decreases the utility of the material. Thus, versatile cost-effective solutions for reducing material dissolution are necessary and PANI has shown to be a promising material in achieving this goal. Not only can PANI coatings reduce material dissolution, reducing unintended contamination of water by dissolved nanomaterials, but they can also improve the metal oxide's photocatalytic properties (34.7% improvement in photocatalysis for the material presented in this work), making the photocatalysts more effective in treating contaminated water. Furthermore, the addition of a magnetic core can ease the recovery of the material after its use, reducing the chances of unintended release of the material in the environment.

2. Experimental

2.1.Materials

The following materials were purchased from Sigma Aldrich: ammonium molybdate tetrahydrate ($(NH_4)_6Mo_7O_{24} \cdot 4H_2O$, AMT), iron (II, III) oxide (Fe_3O_4), nitric acid (12M HNO_3), ethanol, aniline, hydrogen chloride (12M HCl), ammonium persulfate (APS), tetracycline (TC), aluminum chloride, sodium hydroxide, isopropyl alcohol, furfuryl alcohol, terephthalic acid, 2-hydroxyterephthalic acid. Ethylenediaminetetraacetic acid (EDTA) and high-pressure liquid chromatography (HPLC) grade acetonitrile were purchased from (VWR chemicals, Radnor, PA. Potassium dichromate fine crystals and methanol (HPLC grade) were purchased from Fisher Scientific. Tetraacetic acid disodium salt (Ethylenedinitrilo) and Dihydrate (EDTA-2Na) were purchased from Macron Fine Chemicals. L(+) ascorbic acid GR and Tris-HCl ultrapure reagent were purchased from EM Science and J.T. Baker, respectively. Materials were used without further purification.

2.2.Synthesis of PANI coated magnetic MoO_3

Firstly, magnetic MoO_3 was synthesized using a procedure similar to our previous publication [20]. Briefly, 2.46 g ammonium molybdate tetrahydrate (AMT) was dissolved in 20 mL deionized (DI) water. Then, 0.1 g Fe_3O_4 was dispersed in the AMT solution and bath sonicated for 15 minutes to create a homogeneous dispersion using a Bransonic Ultrasonic sonicator. The mixture was heated at 90°C with high stirring (900 rpm) in an oil bath. Finally, 5 mL nitric acid was added slowly to the mixture when it had reached 90 ºC and was left in the oil bath for three hours under continuous stirring to allow the growth of MoO_3. The resulting material was cleaned via magnetic separation first using 70% ethanol and then DI water. The water was removed by centrifugation (Thermo Scientific Sorvall Legend XTR Centrifuge) at 1200 rpm (69 x g) for 40 min and the material was subsequently oven dried at 60°C.

To synthesize the PANI coated material (PANI@MoO_3@Fe_3O_4), a synthesis procedure derived from the synthesis of PANI-CeO_2 [42] was utilized and the optimization of the components of the material were determined previously [27]. An amount of 0.1 mL of aniline was dispersed in 10 mL 2M HCl, and, separately, 234.1 mg of ammonium persulfate (APS) was dissolved in a 10 mL 2M HCl solution. Additionally, 1.012 g of the MoO_3@Fe_3O_4 (MF) material was dispersed in 10 mL 2M HCl and sonicated for 15 minutes. The three solutions were placed in an ice bath to allow their temperatures to equilibrate. Subsequently, the mixture with MoO_3@Fe_3O_4 was allowed to stir using high stirring speed (500 rpm) and the aniline solution was introduced to the mixture. Finally, the ammonium persulfate solution was added dropwise. The resulting mixture was stirred for 2 hours in the ice bath to allow aniline to polymerize on MoO_3@Fe_3O_4. Once the polymerization was complete the PANI@MoO_3@Fe_3O_4 (PMF) material was cleaned with DI water and centrifugation at 1200 rpm (69 × *g*) for 30 min and was then oven dried at 50 ºC overnight [27].

2.3. Characterization

A detailed characterization of the material was conducted in our previous publication [27] in which the PMF was analyzed via scanning electron microscopy (SEM), X-ray diffraction spectroscopy (XRD), X-ray photoelectron spectroscopy (XPS), and attenuated Fourier transform photoelectron spectroscopy (ATR-FTIR). Herein, we provide additional SEM images of the material (samples were coated with gold for 30 s using a Denton Desk V gold coater and the SEM images were acquired using Nova NanoSEM 230), the ζ- potential of the material over a range of pH values, and additional ATR-FTIR data (Nicolet iS10 Mid Infrared FTIR Spectrometer by Thermo Fisher Scientific, USA). To obtain the ζ-potential of the material, first, a stock suspension of 1000 ppm was prepared in DI water. Then, 5 mL of the stock suspension was transferred to a separate container where the pH was adjusted using either 0.1 M HCl or 0.1 M NaOH. The final volume of the pH adjusted suspensions was 10 mL to obtain solutions with 500 ppm of the material. The ζ-potential and hydrodynamic radius were measured at room temperature using dynamic light scattering (DLS) with the Malvern ZetaSizer Nano instrument using the Smoluchowski model. Prior to testing the samples, the ζ-potential and hydrodynamic radius of a Zeta Transfer Standard (ZTS1250, Malvern Panalytical) were measured to ensure proper instrument functionality. All the measurements were performed in triplicate.

2.4. Dissolution

Dissolution experiments were conducted at pH 3, 5, 7, and 10 to determine the relationship between pH and material dissolution for the uncoated and coated materials. DI water at the different pH values was prepared using either 0.1 M HCl or 0.1 M NaOH. Then, either $MoO_3@Fe_3O_4$ (MF) or $PANI@MoO_3@Fe_3O_4$ (PMF) were added to 15 mL of pH adjusted solutions to achieve starting concentrations of 500 ppm of each material. The starting concentration utilized was based on the optimal concentration of the photocatalyst in the photocatalysis process in the degradation of tetracycline by the PMF photocatalyst. Each mixture was kept under static conditions at room temperature. After 35 min (the length of reaction in the photocatalysis experiments) samples were filtered using a 0.2 μm syringe filter (VWR sterile syringe filter). Then, an Amicon centrifugation tube (Ultra-15, Millipore, molecular weight cutoff of 30,000 Da) was utilized to remove any remaining solid particles by centrifuging the solutions for 15 min in a Thermo Scientific Sorvall Legend XTR centrifuge at a speed of 4200 rpm. The resulting solutions were analyzed using a Perkin-Elmer AANalyst 200 Atomic Absorption Spectrometer equipped with a molybdenum lamp [20]. For the instrument calibration, 100 ppm MoO_3 stock solution was prepared by dissolving ammonium molybdate tetrahydrate in DI water, and standard solutions were prepared by diluting the stock solution to 1, 10, 20, 30, and 40 ppm. Since the presence of Fe in the solution can suppress the molybdenum signal, 0.5% aluminum chloride was added to the samples and standard solutions prior to analysis [43]. Samples were prepared in duplicate and tested in triplicate.

2.5. Tetracycline removal

Removal experiments were carried out in a 96 well plate wherein the concentration of tetracycline, photocatalyst, and pH were varied. In a typical experiment, stock solutions of 20 ppm TC in DI water and 1000 ppm of the photocatalyst in DI water were prepared at the target pH by adjusting the pH using either 0.1 M HCl or 0.1 M NaOH. Appropriate amounts of each stock solution were added to two separate 96 well plates and each plate was set in dark conditions by covering with foil to allow initial adsorption of TC to the nanocomposite. The total volume in each well was 200 μL. The PMF concentration was tested at 100 ppm, 200 ppm, 250 ppm, 300 ppm, 500 ppm, 600 ppm, 800 ppm, and 1000 ppm. The initial TC concentration was tested at 1 ppm, 2 ppm, 5 ppm, 8 ppm, and 10 ppm. The pH values utilized were 3, 5, 7, and 10. Due to the high affinity of TC towards the photocatalyst, the plates were set in dark conditions for five minutes. As seen in Figure S1, the adsorption of TC shows no significant change between five minutes and thirty minutes. This higher adsorption capacity with a five minute equilibration time has also been observed with PANI/TiO_2 [36]. After the five-minute adsorption time in the dark, one plate was uncovered and irradiated using visible light (Philips F4T5 soft white, 4W) for 30 minutes. Fluorescence measurements were obtained for each plate prior to irradiation and after 30 minutes using a UV-Vis fluorimeter (Biotek SynergyMX Microtiter plate reader) with an excitation wavelength of 390 nm and an emission wavelength of 520 nm [44]. Experiments were performed in triplicate, and controls containing the tetracycline solution without the PMF material were also included.

2.6. TC Degradation mechanism

To investigate the species responsible for TC photocatalytic degradation, the TC removal experiment at the optimal conditions (500 ppm photocatalyst, 5 ppm initial TC dose, pH 5) was repeated while adding known reactive species scavengers (EDTA as a hole (h^+) scavenger, $K_2Cr_2O_7$ as an electron (e^-) scavenger, isopropanol (IPA) as an OH radical ($\cdot OH$) scavenger, and ascorbic acid (ASC) as a superoxide anion ($\cdot O_2^-$) scavenger) [45]. The concentrations of each scavenger were 10 mM, 50 mM, 75 mM, and 75 mM for EDTA, $K_2Cr_2O_7$, IPA, and ASC, respectively [46,47]. High pressure liquid chromatography (HPLC) was utilized to quantify singlet oxygen ($^1O_2$) production of PMF by degradation of a probe compound (furfuryl alcohol) in the light and dark, as well as for analysis of possible byproducts.

2.7. HPLC procedures

2.7.1. Singlet oxygen detection

A previously reported method was utilized in the evaluation of the singlet oxygen ($^{1}O_2$) species [20]. PMF (500 ppm), as described in the photocatalysis section, was mixed with 10 μM furfuryl alcohol (FFA), and the same experimental procedure as the TC degradation experiments was performed. Blank (with PMF only) and negative controls (without PMF and only FFA) were also prepared. After the 30 min reaction, the PMF was removed by filtration using 0.05 μm nylon filters. High performance liquid chromatography (HPLC) was utilized for the analysis of the filtrate samples using an Agilent Technologies 1290 Infinity HPLC with a Zorbax Eclipse Plus C18 (4.6 × 150 mm, 5 μm). The mobile phase was 80% H_2O: 20% MeOH, 1 mL/min was used as the total flow rate, and the injection volume was set to 20 μL. $^{1}O_2$ was determined via quantification of the FFA using the UV peak area for λ = 219 nm (retention time of 2.6 min) and the %FFA degradation was calculated by the equation

$$FFA\ (\%) = \frac{Negative\ control\ concentration - Sample\ concentration}{Negative\ control\ concentration} \times 100 \qquad (1)$$

An FFA calibration standard was prepared and analyzed using HPLC with the same conditions.

2.7.2. Tetracycline quantification

The HPLC analysis for the quantification of tetracycline and degradation byproducts was carried out on the same Agilent 1290 Infinity HPLC system used for the FFA analysis. All the samples were filtered using 0.1 μm PVDF syringe filter (Durapore, Merck Millipore, Carrigtwohill Co., Cork, Ireland) prior to injection. The sample injection volume was 20 μL and flow rate was 0.5 mL min^{-1}. The gradient method was optimized on mixtures of tetracycline and several of its degradation byproducts (4-epitetracycline, oxytetracycline, tetracycline, methacycline, doxycycline, chlortetracycline, minocycline, and anhydrotetracycline) to allow for the separation and quantification of a variety of compounds (Figure S2) [48–51]. A gradient elution was used for a 30 min total run duration using mobile phase (A) 0.001 M ethylenediaminetetraacetic acid (EDTA) in deionized water and (B) HPLC grade acetonitrile (VWR chemicals, Radnor, PA). The mobile phase composition was ramped from 90% A (10%B) to 85% A (15% B) over the first 3 minutes, then ramped to 75% A (25% B) over the next 12 minutes, and finally ramped to 50% A (50% B) over 10 minutes. Then, the composition was ramped back to 90% A (10% B) over 2 minutes and held for 3 minutes to equilibrate for the next injection. Tetracycline was quantified using the UV peak area at 355 nm as the peak wavelength.

2.8. Statistical analysis and chemical structures

Statistical analysis was performed using the software Prism 9 utilizing two-way ANOVA analysis with multiple comparisons (correcting for multiple comparisons using the Bonferroni test). 2-D chemical structures were drawn using MarvinSketch Version 21.9 by ChemAxon, and 3-D molecules used in illustrations were created using Avogadro: an open-source molecular builder and visualization tool, Version 1.2.0. Illustrations were created using Affinity Designer Version 1.9.3.

3. Results and Discussion

3.1. Material Characteristics

The SEM images (Figure 1) of the uncoated $MoO_3@Fe_3O_4$ (MF) displayed a hexagonal rod type structure (Figure 1.a) with rod diameters ranging from approximately 0.24 to 1.25 μm [27]. The

MF material presented a smooth surface, which changed once coated with the emeraldine salt form of PANI. The surface appeared rough after the coating process indicating the presence of the polymer in the PANI@MoO_3@Fe_3O_4 (PMF) material (Figure 1.b). The polymer layer appeared to cover the majority of the MF surface and was determined to have a radius of gyration of 136.9 ± 0.92 nm using small-angle neutron scattering data analysis in our previous publication, which examined the growth of the polymer layer on the nanoparticles [27]. The measured hydrodynamic radius of the material changed from 794.90 ± 15.13 nm to 889.20 ± 12.02 nm when coated with PANI, and its polydispersity decreased from 0.477 to 0.449. The PANI coating was determined to have a significant effect on the dissolution of the MoO_3 in the material (Figure 2). MF exhibited significant dissolution of MoO_3 as pH was increased from 3 to 10 reaching a maximum dissolution of 22.9 ± 1.0% at pH 10. The PANI coating was able to reduce this dissolution to a maximum of 5.6 ± 0.2%. In the MF material, dissolution at pH 3 was determined to be 2.9 ± 0.1% (100 ppm difference from the dissolution of the MF material at pH 10), while in the PMF material, the dissolution at pH 3 was 1.6 ± 0.2% and increased significantly less than that of the MF material as pH was increased to 10 (20 ppm increase). Overall, pH increased dissolution in the coated and uncoated materials, however, the effect of pH in the dissolution of the material was significantly reduced (76% reduction at pH 10) with the presence of the PANI coating.

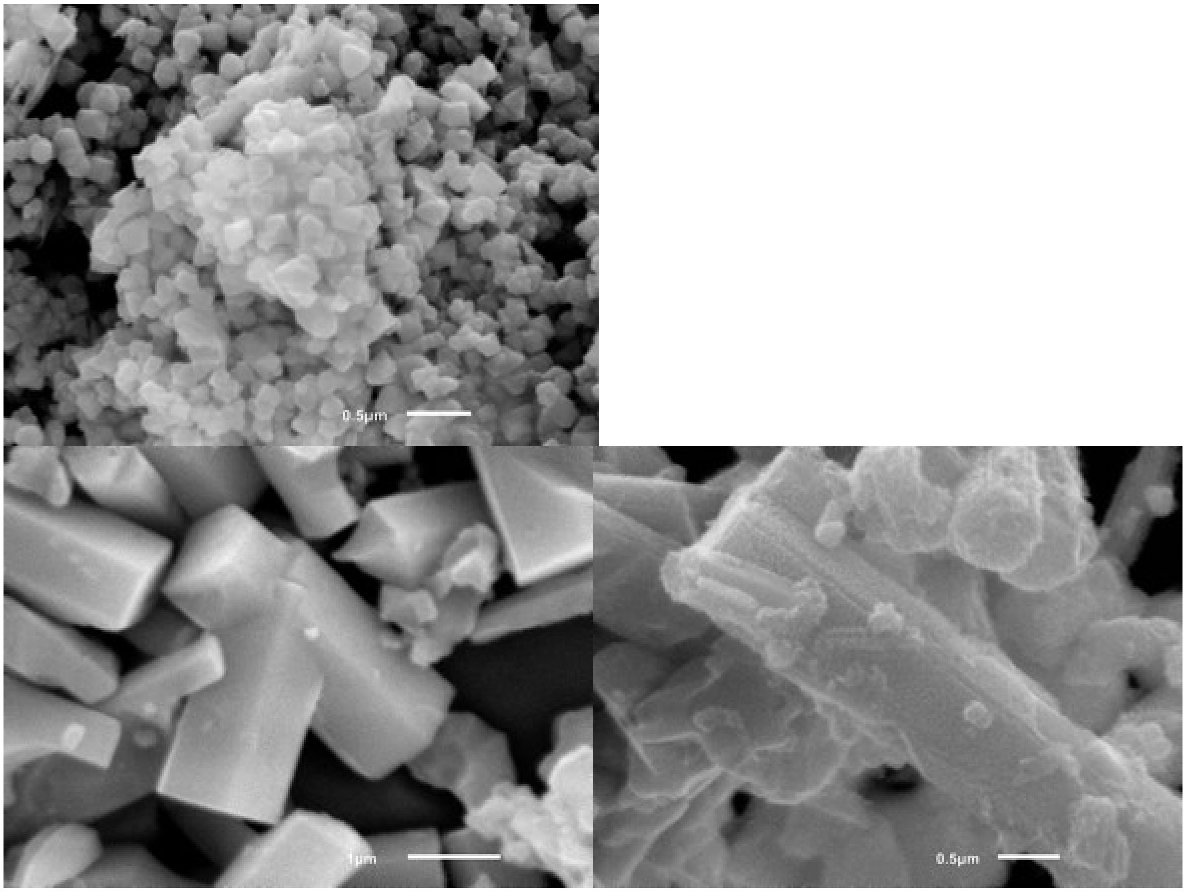

Figure 1: SEM images of a) Fe_3O_4 (× 27,000 magnification), b) MF (× 20,000 magnification), and c) PMF (× 27,000 magnification)

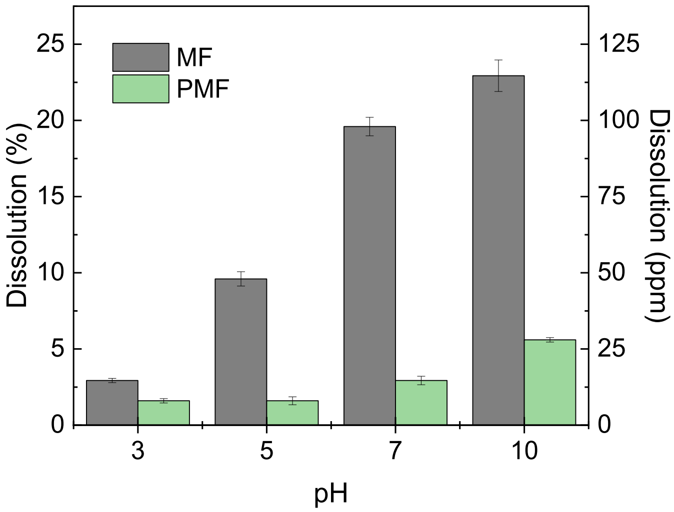

Figure 2: Dissolution of uncoated magnetic MoO_3 (MF) and PANI coated magnetic MoO_3 (PMF)

The ζ-potential of the PMF material was measured at a wide pH range, with pH values in the range of 1 to 11 (Figure S3) and the isoelectric point (IEP) was estimated to have a value of 7.44 ± 0.21. At more acidic pH values, the material was positively charged in solution, and as pH increased the effective surface charge of the material decreased. Likely, at more basic pH values the emeraldine salt started to change to emeraldine base, which reduced the number of protonated nitrogen groups in the PANI backbone (Scheme 1) [52,53]. Due to this change, the overall surface charge and conductivity were expected to decrease as pH increased.

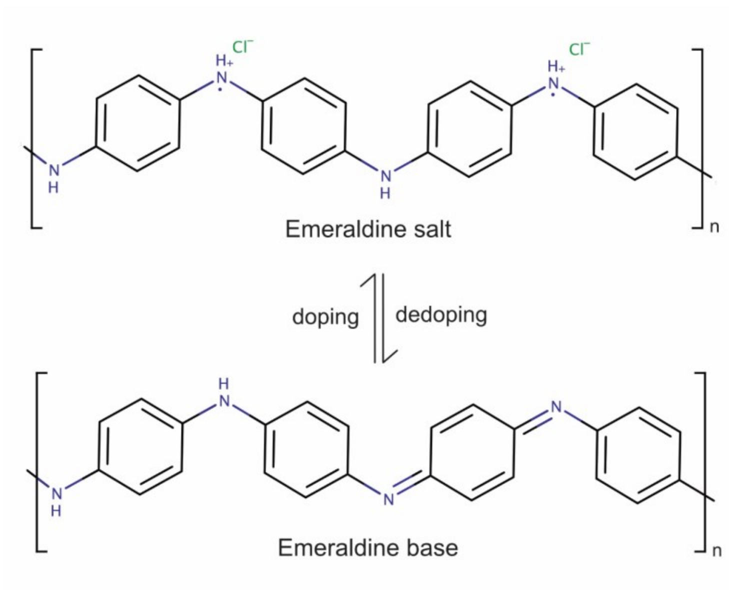

Scheme 1: PANI doped (emeraldine salt) form and deprotonated form (emeraldine base) [54]

3.2. Photocatalytic activity

To determine the conditions that led to high photocatalytic activity, the effects of changes in photocatalyst dosage, initial TC concentration, and pH level were examined (Figure 3 presents the photocatalysis results, which is also supported by the HPLC data in Figure S1). Photocatalytic activity is defined herein as TC removal solely due to degradation induced by light exposure. Removal in the light is a result of adsorption, photocatalysis, and any catalytic processes, while removal of TC in the dark is a result of only adsorption and any Fenton reactions or catalytic processes that could be potentially occuring [20]. Photocatalytic activity largely depends on the ability of the material to promote reactive oxygen species (ROS) generation since they are ultimately responsible for the degradation of TC. The primary species leading to TC degradation by a variety of materials are OH radicals (·OH) and superoxide radicals ($\cdot O_2^-$), with holes (h^+) also playing a role in the mechanism [55]. To help with the investigation of the mechanism of TC degradation by PMF, optimal reaction conditions were first determined.

As the TC concentration was kept constant and the photocatalyst dosage increased from 100 to 1000 ppm, TC removal showed an upward trend (Figure 3.a). In addition, while removal values initially increased, eventually they reached a plateau, where the incremental increases in dosage did not show statistically significant changes in the removal values of TC in light and dark (Table S1). The initial increase in photocatalytic activity can be attributed to the increase of PMF concentration. It has been found that an increase of the photocatalyst in solution increases photocatalytic and adsorption active sites and as a result increases the photogenerated reactive oxygen species responsible for TC degradation [56]. However, as photocatalyst concentration increased so did the turbidity of the solution. An increase in turbidity limited the light from reaching the material, effectively reducing the photocatalytic activity [9,56]. The minimum effective concentration of PMF in which TC removal in dark and light did not show statistically significant changes with the incremental increases in photocatalyst concentrations, but showed a statistically significant difference between light and dark TC removal (p *value* = 0.013), was 500 ppm. At this concentration TC removal reached 63.6 ± 0.04% in the light and 54.4 ± 1.2% in the dark.

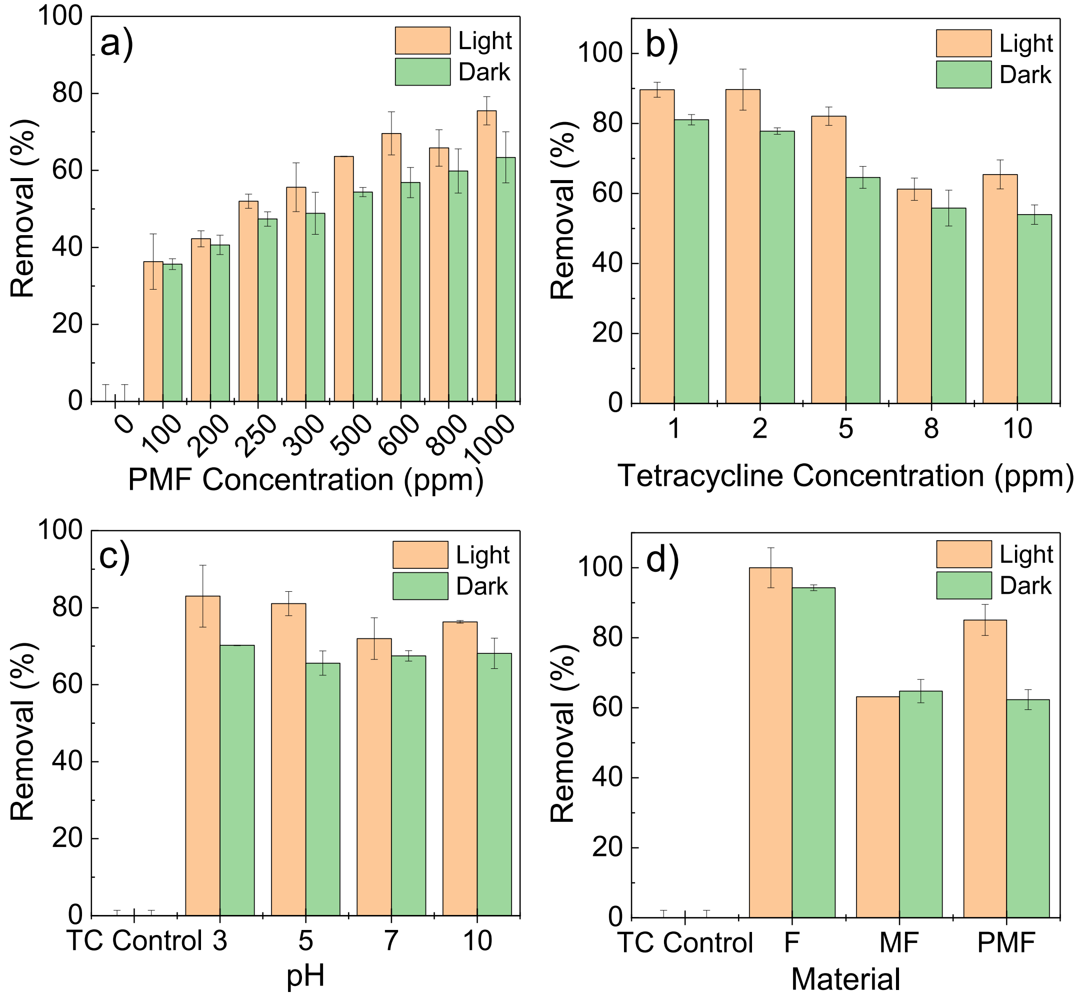

Figure 3: Removal of TC in light and dark determined using fluorescence quantification when (a) PMF is increased and TC concentration is kept at 10 ppm at pH 5, (b) TC concentration is altered and PMF concentration is kept at 500 ppm at pH 5, (c) PMF concentration is 500 ppm and TC concentration is 5 ppm and pH is varied, and (d) comparing removal of TC between each synthesis stage of the material (F is Fe_3O_4, MF is MoO_3 coating the Fe_3O_4, and PMF is the PANI coated MF) using 500 ppm of each material and 5 ppm TC at pH 5

When TC concentration was increased from 1 to 10 ppm with the optimum photocatalyst concentration of 500 ppm (Figure 3.b), the TC concentration, which showed the highest photocatalytic degradation (removal of TC in the light not including adsorption), was 5 ppm (82.1 ± 2.6% removal in light and 64.6 ± 3.2% removal in the dark, corresponding to 8.2 mg TC/g photocatalyst and 6.4 mg TC/g photocatalyst, respectively) with a p value less than 0.0001 when comparing TC removal in the light and in the dark. The reaction best followed a pseudo first order reaction where the rate constant, k, was calculated from the HPLC data (Figure S1) to be 3.7×10^{-2} min^{-1}. Removal of TC was greatly reduced and the differences between TC removal in light and dark were largely insignificant when TC initial concentrations were larger than 5 ppm. Likely, as TC increased, the surface of PMF reached its adsorption capacity and the additional TC hindered light absorption by PMF by its excess presence in solution, which could have caused complexation with other TC molecules on the surface of the material. It is also likely that the excess TC led to an increase in degradation intermediates, which could have competed for ROS thus hindering the breakdown of TC [57].

The change in photocatalytic activity as pH became more alkaline (Figure 3.c) can be attributed to the effect of pH changes on TC and PANI. TC exhibits electron donor and acceptor moieties, and at a pH of approximately 6, it aquires a zwitterionic form (Scheme 2) [58]. For photocatalysis to occur, TC needs to be adsorbed to the surface of the photocatalyst. Adsorption of TC is highest when the adsorbent is a good electron donor [59]. As evidenced in Figure 3.c, adsorption did not change significantly as pH increased, although photocatalytic activity diminished when pH was 7 and higher, likely, due to the chemical changes occuring in both TC and PANI as pH increased (see Figure S2, Scheme 1, and Scheme 2). As pH increased, deprotonation of emeraldine PANI occurred, thus, changing PANI to its emeraldine base form (Scheme 1) and reducing its surface charge as discussed in section 4.1 [52]. The protonation of PANI is what improves conductivity due to the polarons and bipolarons that are formed and act as charge carriers [52]. The emeraldine base form of PANI is non-conductive, which can hinder electron mobility. It has been shown that PANI in its conductive form improves photocatalytic activity by reducing e^{-}-h^{+} recombination at valance and conduction bands of the metal oxide [33]. In a study on the effect of PANI coatings on TiO_2 for the degradation of azo dye, it was determined that pH changes alter the degradation rate, while the removal amount is not changed [33]. In another study examining the triethylamine (TEA) adsorptive properties of PANI coated α-MoO_3, it was determined that reduction in conductivity of PANI hinders hole transport around the interface due to the disruption of the junction's e^--h^+ equilibrium [59]. The result is an increase in the depletion region width, which can prevent hole transport in the juncton [59]. Thus, the recombination of e^-- h^+ pairs of the metal oxide photocatalyst increases, effectively reducing photocatalytic activity.

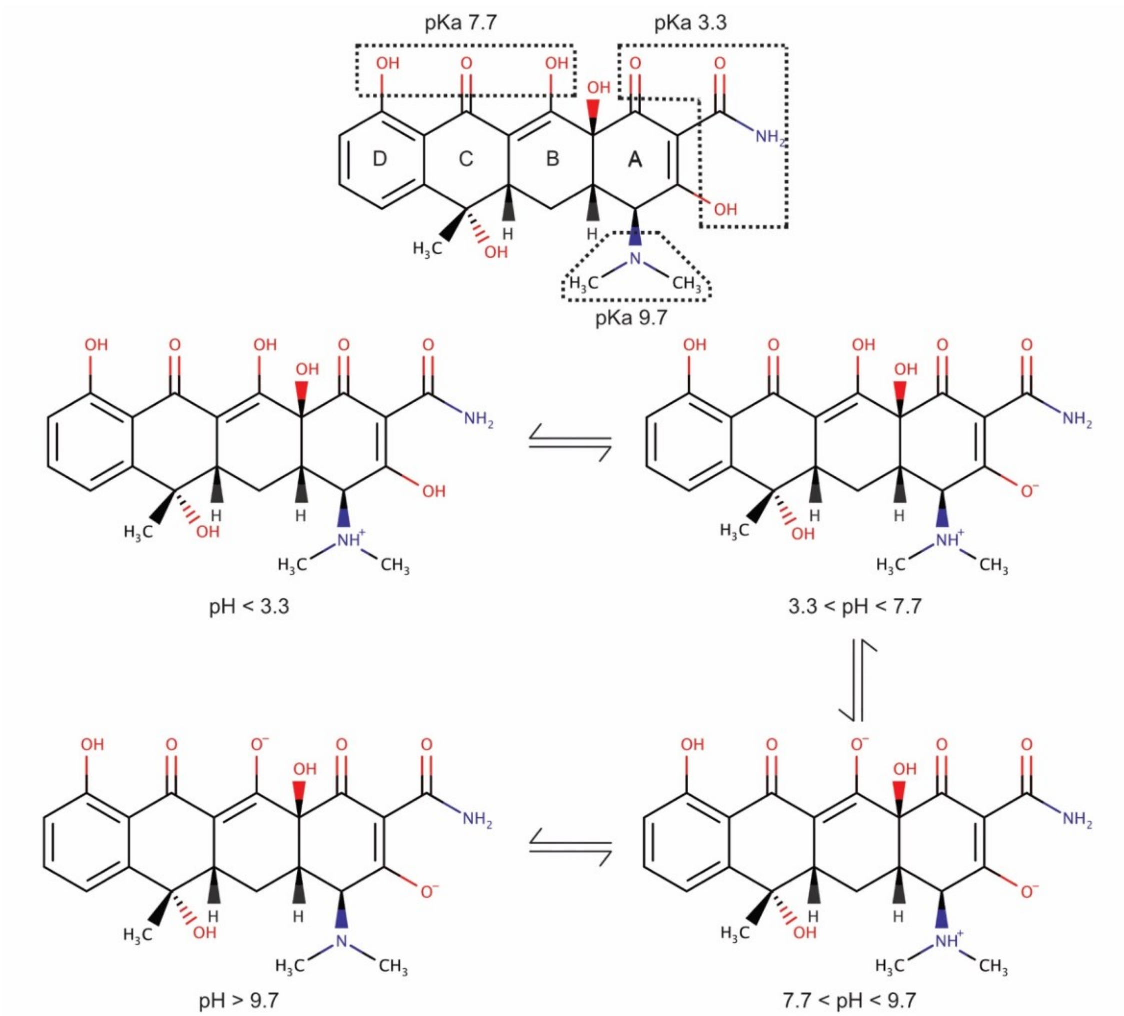

Scheme 2: TC dependence on pH

When comparing removal of TC with the coated and uncoated material (Figure 3.d) it is evident that PANI is critical in improving the photocatalytic activity of the material in the degradation of TC. Conductive polymers in general have demonstrated their role as stable photo-sensitizers due to their charge carrier separation efficiency [35]. For PANI, its synergistic effect on semiconducting material has been observed to arise from its ability to form heterojuction interfaces via the generation of trapping levels [35]. In a study of the effect of PANI on CdS, for instance, photoexcited electrons from PANI were shown to move to conduction band of the photocatalyst, and, in turn, the photogenerated holes from the photocatalyst were able to move to the surface of the composite thereby reducing the probability of recombination of electrons and holes [35]. In PANI-TiO_2, it was speculated that in addition to the decrease in e^--h^+ recombination, PANI also protected the TiO_2 surface from being blocked by intermediates owing to the mobility of PANI active sites [33]. It has been previously shown that the presence of MoO_3 in PANI enhances the conductivity of PANI via the emergence of trapping levels [59,60]. This heterojunction formation has been shown to improve the adsorptive capabilities of α-MoO_3/PANI composite towards triethylamine (TEA) [59]. The α-MoO_3 component acts an n-type semiconductor while PANI acts as a p-type in the p-n heterojuction, which was favorable in the physisorption of vapors that are good electron donors, such as the TEA studied [59]. In the case of the PMF material tested herein, while it is possible PANI prevented byproducts from taking up active sites, the reduction of e^--h^+ recombination and the movement of holes to the surface of the material where likely the primary contributing factors in the observed increase in photocatalytic activity. Comparing the photocatalytic performance of PMF with other materials when tested in the degradation of tetracycline (Table 1) shows that the PANI coated material used in this study has significant advantages. While other photocatlysts use UV light to degrade TC, PMF can degrade TC using low power visible light. In addition, the time it takes to reach over 80% degradation of TC (30 min) is significantly less than other materials and does not require a large quantity of catalyst to degrade 5 ppm TC.

Table 1: Photocatalytic degradation performance of the material presented in this work and of other materials for comparison

Material	**[Catalyst] (ppm)**	**Initial TC dose (ppm)**	**Light Source**	**TC removal and Reaction time**	**Removal rate constant ($\times 10^{-2}$ min^{-1})**	**Ref**
Bi_2O_3/Bi_2S_3	3000	5	Visible	84% (60 min)	-	[61]
LaCoO3:Bi4Ti3O12	500	5	UV-Vis	87.8% (100 min)	2.2	[62]
TiO_2-P25	200	10	Visible (500 nm)	56.7% (120 min)	0.69	[63]
$Zn_4B_6O_{13}$	1600	20	UV, 125W	89% (180 min)	0.67	[64]
ZnO_e	10	5	UV-Vis, 60 W	75% (180 min)	1.04	[65]
PANI@MoO_3@Fe_3O_4	500	5	Visible, 4W	82.1% (30 min)	3.70	This work

The ATR-FTIR spectra of TC and PMF in the light and dark with and without TC were acquired to confirm the adsorption and degradation of TC by PMF and examine whether the chemistry of PMF was affected by light. The wide-range spectra (4000 cm^{-1} to 675 cm^{-1}) are shown in Figure S4.a, however, the spectra were primarily analyzed in the range below 1750 cm^{-1} (shown in Figure 4 with more detailed spectra shown in Figure S4) since the characteristic peaks of TC are in the range of 1700 to 1200 cm^{-1} [66,67]. The spectra between 3100 cm^{-1} and 2870 cm^{-1} are also included due to the presence of a peak at 2981 cm^{-1} in the PMF Light and Dark without TC spectra, which was attributed to the C-H stretching vibrations of PANI [68]. In comparing the PMF ATR-FTIR spectra after the material has been under dark conditions and after it has been irradiated by visible light for 30 minutes, no discernible difference between the spectra was observed, indicating that there was no significant degradation of PANI in the light (Figure 4). This stability of PANI under visible light in conjunction with the lower material dissolution observed after coating the material with PANI are favorable properties when considering the efficiency and recyclability of the material. However, additional studies would need to be conducted to examine in depth the long term stability and recyclability of the material.

The TC spectra in Figure 4 presented two peaks in the 3100 cm^{-1} and 2870 cm^{-1} range at 3036 cm^{-1} and 2950 cm^{-1} attributed to the C-H and $-CH_3$ stretching, respectively [69,70]. In the TC spectra, the peaks at 1693 and 1612 cm^{-1} corresponded to the C=O stretching vibrations in the carbonyl in the amide group of ring A and carbonyl group of ring A of TC, respectively [67,71,72]. The spectra of PMF with TC are very similar to that of PMF in the light and dark aside from the appearance of three additional distinct bands, indicating that the adsorption of TC primarily occured at the surface of PMF [73]. The emergence of the peak at 1644 cm^{-1} corresponding to C=O stretching vibrations after TC adsorption on PMF was likely a peak shift from the 1693 cm^{-1} peak of TC, indicating the presence of hydrogen bonding between the amide group of TC and the surface of PMF [66,74,75]. The peak of TC at 1318 cm^{-1} and of PMF at 1300 cm^{-1} from the C-N stretching in the amide group and C-N/C-N^+ stretching vibrations, respectively, appearred to shift to the strong peak at 1278 cm^{-1}, which was present in the PMF + TC in the dark spectra [27,67,73]. The peak at 1278 cm^{-1} was likely due to hydrogen bonding interactions between the C-N of the TC amine group and C-N/C-N^+ of PANI. Furthermore, there were changes in the C-H vibrations of the TC and PMF spectra after TC adsorption. The C-H bending vibrations of TC at 829 cm^{-1} shifted to 837 cm^{-1} in the PMF + TC dark spectra. Given these changes, TC likely formed strong hydrogen bonds with the PANI coating at the TC amino, carbonyl, or C-H groups as shown in Figure 5. Upon light irradiation of the PMF + TC the peak at 837 disapeared, the and the C=O stretching vibrations and C-N vibrations decreased in intensity. Given that the difference between PMF in the dark and PMF in the light was insignificant, the ATR-FTIR spectra changes signified a decrease in the presence of TC on the surface of PMF indicative of TC degradation.

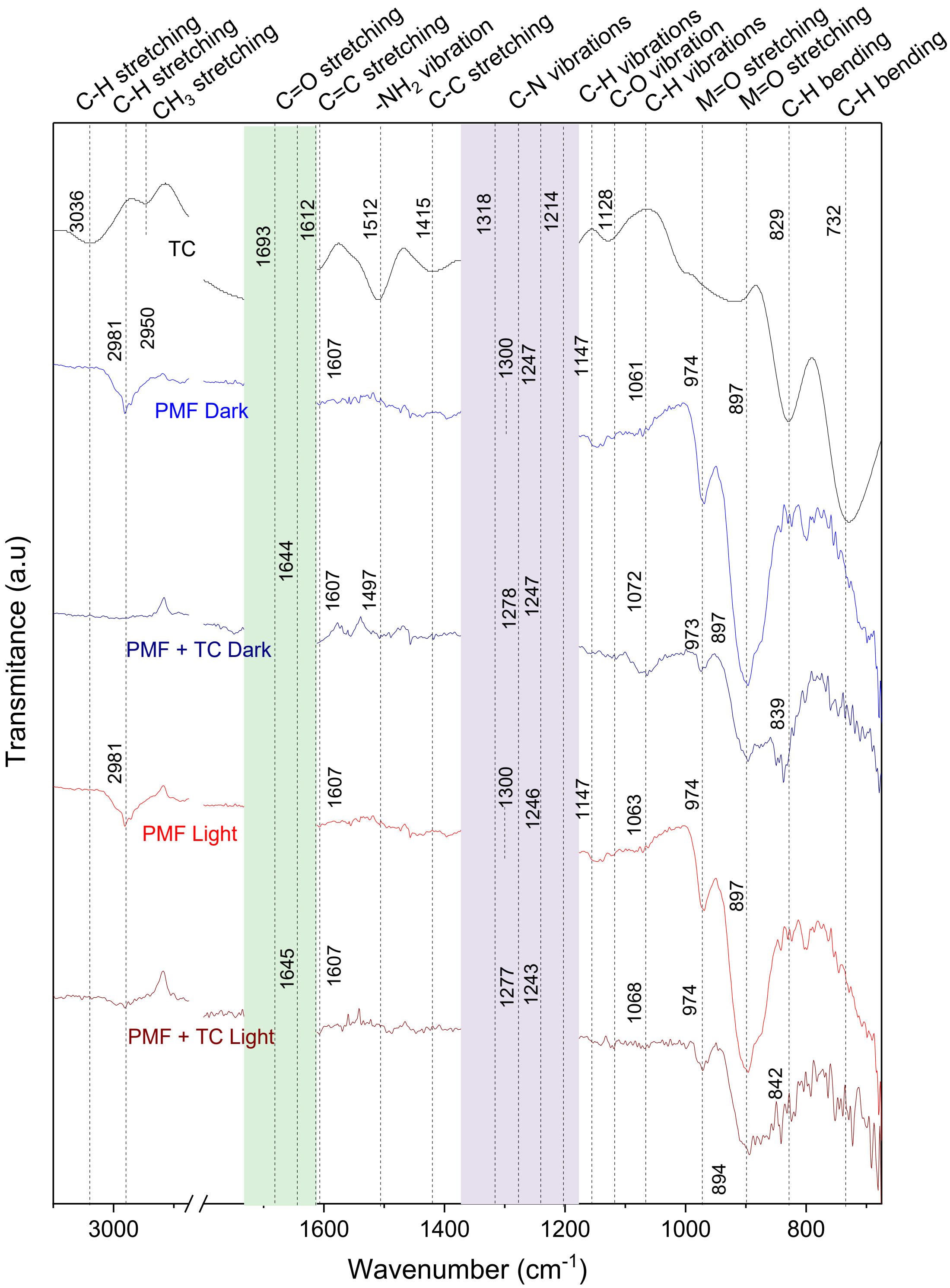

Figure 4: ATR-FTIR spectra of TC and TC adsorbed on PMF after 30 minutes in the dark and 30 minutes in the light

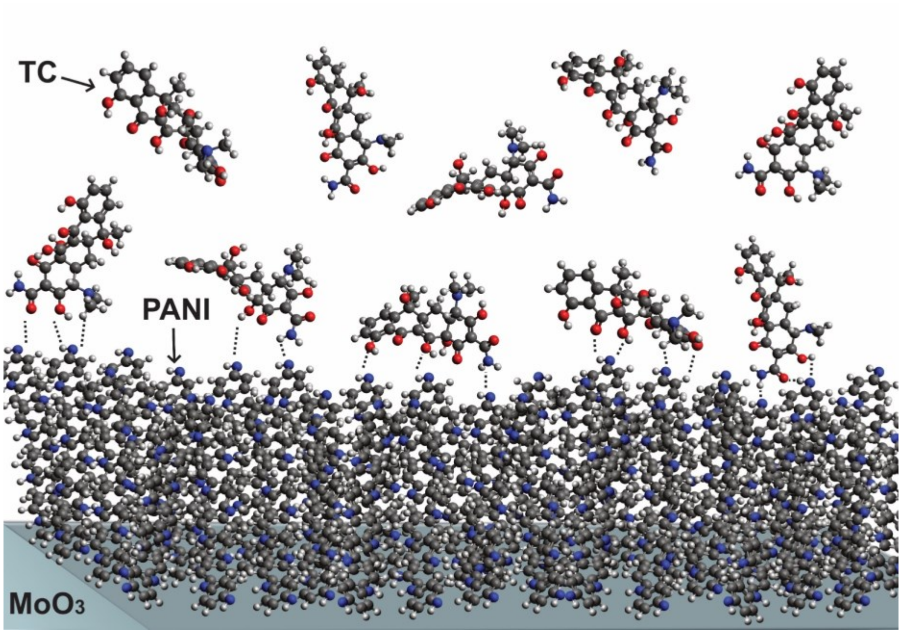

Figure 5: PMF and TC interaction based on ATR-FTIR analysis. TC primarily forms hydrogen bonds at the TC amide functional group and C-H and C=O along the structure

3.3. ROS involvement in TC degradation

To elucidate the probable mechanism of photodegradation of TC by PMF, photocatalysis experiments were conducted in the presence of reactive species scavengers. In particular, EDTA was utilized as a hole (h^+) scavenger, $K_2Cr_2O_7$ as an electron (e^-) scavenger, isopropanol (IPA) as a hydroxyl radical (·OH) scavenger, and ascorbic acid (ASC) as a superoxide anion ($\cdot O_2^-$) scavenger [45]. In addition, singlet oxygen production and presence of TC and several TC products were evaluated using HPLC. The TC degradation results from HPLC agreed with the results from the fluorescence spectroscopic analysis. HPLC chromatograms (see Figure S2 and Figure S5) were utilized to calculate the TC concentration progression in light and dark during its photocatalysis by PMF (Figure S1) and assess TC products. The HPLC analysis on the byproducts did not reveal any other TC conformations or degradation byproducts. Figure S2 shows the tetracycline products (4-epitetracycline, oxytetracycline, tetracycline, methacycline, doxycycline, chlortetracycline, minocycline, and anhydrotetracycline) tested to compare with the TC degradation samples in the

30 min run [48–51]. While not every possible byproduct was able to be tested for identification, peaks in the HPLC data, other than TC, were too small to accurately ascertain their presence (see Figure S2 and Figure S5). Thus, either minute amounts of byproducts were generated in the solution, or any byproducts were adsorbed by the PMF, which would be beneficial in water treatment as any toxic byproducts would be prevented from being released.

Via the scavenger experiments, we can propose likely mechanisms of TC degradation by observing effects of ROS quenching by the scavengers on the photocatalysis of TC [14,15,57,76]. As all scavengers, aside from $K_2Cr_2O_7$, eliminated any TC removal due to light absorption (Figure 6a). From this data, we can conclude that the critical reactive species responsible for the photodegradation of TC were photogenerated h^+, $\cdot OH$, and $\cdot O_2^-$. Specifically, since no change in adsorption and no photocatalysis were observed when the h^+ scavenger (EDTA), the $\cdot OH$ scavenger (IPA), and the $\cdot O_2^-$ scavenger (ASC) were in the solution, all respective quenched reactive oxygen species participated in the degradation mechanism of TC by PMF. While some catalytic activity is possible in the dark as evidenced by the presence of less than 5% FFA removal by $^1O_2$ generation, the increase in singlet oxygen production in the light indicates a greater amount of $^1O_2$ production in the light (Figure 6b). Generation of $^1O_2$ can result from oxidation of $\cdot O_2^-$, which forms via a stepwise procedure initiating when water molecules are oxidized to form $\cdot OH$ or H_2O_2 [77]. The hydroxyl radicals can then dimerize to form H_2O_2, which can then be oxidized into $\cdot O_2^-$ [77]. In essence, ROS formation can follow either of these following reactions:

$$H_2O + h^+ \xrightarrow{oxidation} {}^{\bullet}OH \xrightarrow{dimerization} H_2O_2 \xrightarrow{oxidation} {}^{\bullet}O_2{}^- \xrightarrow{oxidation} {}^1O_2 \qquad (2)$$

or

$$H_2O + h^+ \xrightarrow{oxidation} H_2O_2 \xrightarrow{oxidation} {}^{\bullet}O_2^- \xrightarrow{oxidation} {}^1O_2. \quad (3)$$

Given that TC photocatalytic degradation was hindered by all three scavengers, it is likely TC degradation by PMF was primarily achieved via nucleophilic attacks by $\cdot O_2^-$ and $\cdot OH$ formed via the oxidation of water molecules. The significant role of $\cdot O_2^-$ and $\cdot OH$ in TC degradation has also been observed in the degradation of TC by CuS_4 and by the use of electro-catalysis [55,57]. However, in the TC degradation by PMF, h^+ also plays a critical role as evidenced in Figure 6, either via its participation in the formation of $\cdot O_2^-$ and $\cdot OH$ or in the TC degradation pathway. One potential degradation pathway, in which $\cdot O_2^-$ and $\cdot OH$ were the primary reactive species, was observed when CuS_4 was utilized [55]. In this reaction, TC reacted with $\cdot O_2^-$ and $\cdot OH$, resulting in the cleavage of -NH and inclusion of $\cdot OH$, respectively [55]. Subsequent attacks by $\cdot O_2^-$ and $\cdot OH$ resulted in cleavage of the -CO group or addition of $\cdot OH$ in the new products, respectively, leading to ring opening and eventual breakdown of the intermediate products by reactive species (Figure 7) [55]. In the electro-catalytic degradation of TC by a carbon nanotube/agarose/indium tin oxide electrode, $\cdot O_2^-$ and $\cdot OH$ also played major roles in the degradation of the TC molecules [57]. It was speculated that $\cdot OH$ first reacted with TC areas high in electron density, and then was oxidized, primarily by $\cdot O_2^-$, forming three main intermediates, which were further degraded by the elimination of ketone groups, carboxylic groups, and ring opening reactions [57]. In the visible-light photodegradation of TC by BiOCl@CeO_2 microspheres, $\cdot OH$ were thought to directly oxidize TC after being generated via the oxidation of OH^- or H_2O by h^+ in the BiOCl valence band [76]. In addition, $\cdot O_2^-$, formed by e^- capture of O_2 in the conduction band of CeO_2, was thought to also play a role in degradation mechanism by oxidizing TC [76]. Quenching of any step in the different degradation mechanisms would lead to the preservation of the TC molecule or byproduct structures.

In the case of PMF degradation of TC, the generation of $\cdot O_2^-$ and $\cdot OH$ was most likely initiated by the oxidation of water by h^+ in the valence band of PANI, as in the case of the BiOCl@CeO_2 microspheres. Then, nucleophilic and radical attacks by $\cdot O_2^-$ and $\cdot OH$ could have been responsible for the degradation of TC. We should note that $\cdot O_2^-$ could also have formed via the reduction of O_2 by photoexcited e^-, where in this pathway $\cdot O_2^-$ could become reduced to H_2O_2, and then $\cdot OH$, leading to the breakdown the structure of TC. However, since the addition of EDTA to the reaction had little effect on the photocatalytic activity of PMF, photogenerated e^- do not appear to play a significant role in this reaction. This was expected as ROS generation takes place at the surface of the material and PANI exhibits p-type semiconducting properties when paired with MoO_3, making holes the more probable reactive species in the initiation of the photodegradative process.

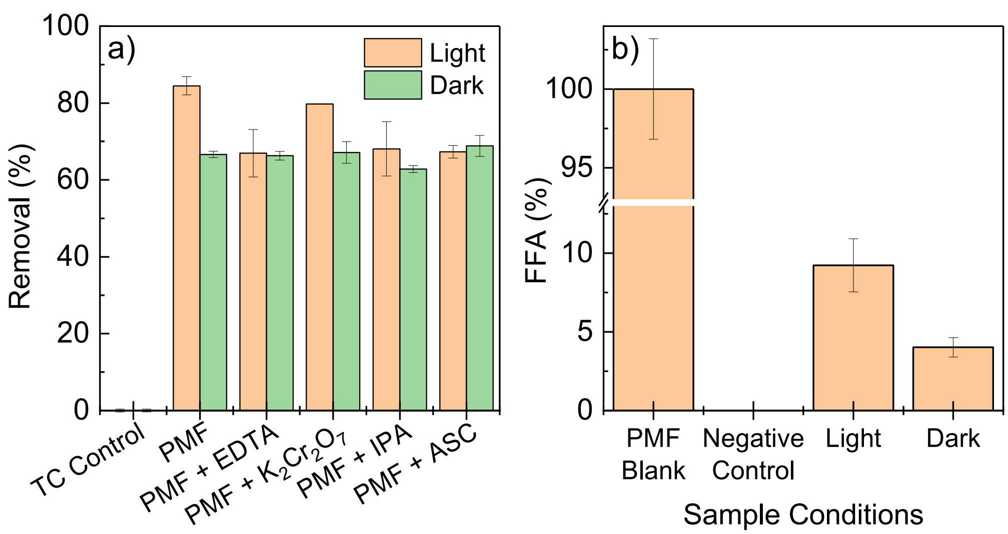

Figure 6: a) Effect of the addition of ROS scavengers on PMF TC removal where TC alone was used as a control and b) Singlet oxygen determination from FFA production by PMF in the light and dark.

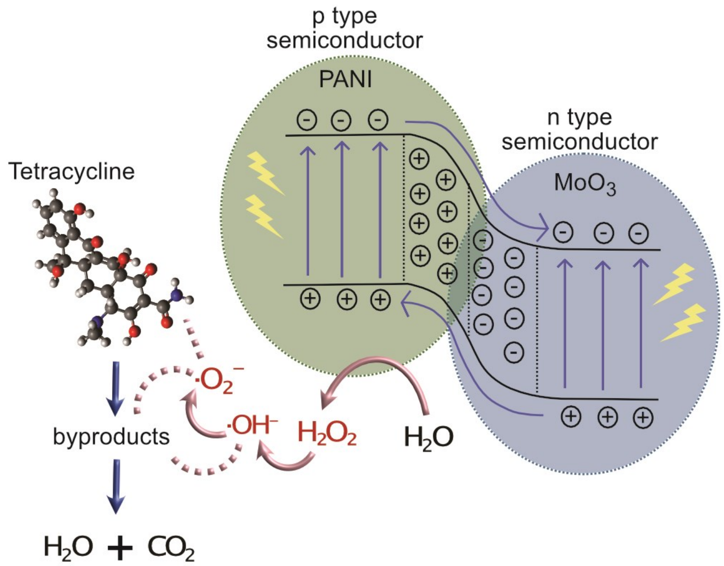

Figure 7: Potential mechanism of photocatalytic degradation of TC by PMF

4. Conclusion

In the investigation of PANI coated magnetic MoO_3 for photocatalysis of TC, the effect of the PANI coating on photocatalytic activity and dissolution were determined. The conductive and stabilization capabilities of PANI allowed for the reduction of dissolution and improvement in photocatalytic activity of the magnetic MoO_3. While PANI increased photocatalytic activity in pH 3 through pH 10 solutions, in pH 7 and above, a reduction of TC degradation was observed, likely due to the loss of conductivity as PANI transitions from its emeraldine salt to emeraldine base forms. At the optimal solution conditions (pH 5, 500 ppm PMF concentration, and an initial TC concentration of 5 ppm), the PMF material improved photocatalytic activity by more than 20% when exposed to visible light for 30 minutes. The primary reactive species responsible for TC degradation were likely the superoxide anion and hydroxyl radical. Their generation hinged on the production of photogenerated holes by the material and subsequent ability to oxidize water molecules and continue the oxidation process until the formation of superoxide anions and hydroxyl radicals. Given the type of ROS produced, a likely mechanism of TC photodegradation involves cleavage of the -NH and -CO group, ring opening, and breakdown of the smaller molecules generated. The lack of direct involvement of photoexcited electrons in ROS generation was attributed to heterojunction formation and the role of PANI as the p-type material of the p-n semiconductor. Furthermore, the MoO_3 material was stabilized via the considerable reduction in its dissolution across the pH range tested (pH 3 to 10) once coated with PANI. While substantial TC removal and photodegradation within 30 minutes was demonstrated, the solution had optimal conditions. To truly assess the usability of PMF in water treatment, additional studies must be conducted examining the photodegradative ability of the material when in complex solutions (multiple contaminants, ions, organic matter, among other substances) as well as the reusability of the material. However, this study effectively provides an initial assessment of the material and elucidates its potential photodegradation mechanism.

Abbreviations

APS: Ammonium Persulfate

ASC: Ascorbic acid

EPC: Emerging pharmaceutical contaminant

IPA: Isopropanol

ROS: Reactive oxygen species

TC: Tetracycline

PANI: Polyaniline

PMF: PANI@MoO_3@Fe_3O_4

Acknowledgments

This work was supported by the NSF BEINM grant (Grant Number: 1705511)), the Welch Foundation award number (E−2011-20190330), and the Engineering Research and Development for Technology (ERDT) Sandwich Program of the College of Engineering, University of the Philippines, Diliman. The findings achieved herein are solely the responsibility of the authors.

1. References

[1] S.K. Fanourakis, J. Peña-Bahamonde, P.C. Bandara, D.F. Rodrigues, Nano-based adsorbent and photocatalyst use for pharmaceutical contaminant removal during indirect potable water reuse, Npj Clean Water. 3 (2020) 1. doi:10.1038/s41545-019-0048-8.

[2] T. Velempini, E. Prabakaran, K. Pillay, Recent developments in the use of metal oxides for photocatalytic degradation of pharmaceutical pollutants in water—a review, Mater. Today Chem. 19 (2021) 100380. doi:10.1016/j.mtchem.2020.100380.

[3] Z. Cai, Y. Song, X. Jin, C.-C. Wang, H. Ji, W. Liu, X. Sun, Highly efficient AgBr/h-MoO3 with charge separation tuning for photocatalytic degradation of trimethoprim: Mechanism insight and toxicity assessment, Sci. Total Environ. 781 (2021) 146754. doi:10.1016/j.scitotenv.2021.146754.

[4] Y. Hong, C. Li, G. Zhang, Y. Meng, B. Yin, Y. Zhao, W. Shi, Efficient and stable Nb2O5 modified g-C3N4 photocatalyst for removal of antibiotic pollutant, Chem. Eng. J. 299 (2016) 74–84. doi:10.1016/j.cej.2016.04.092.

[5] K. Rabé, L. Liu, N.A. Nahyoon, Y. Zhang, A.M. Idris, J. Sun, L. Yuan, Fabrication of high

efficiency visible light Z-scheme heterostructure photocatalyst g-C 3 N 4 /Fe 0 (1%)/TiO 2 and degradation of rhodamine B and antibiotics, J. Taiwan Inst. Chem. Eng. 96 (2019) 463–472. doi:10.1016/j.jtice.2018.12.016.

[6] M. Szkoda, K. Trzciński, A.P. Nowak, M. Gazda, M. Sawczak, A. Lisowska-Oleksiak, The effect of morphology and crystalline structure of Mo/MoO3 layers on photocatalytic degradation of water organic pollutants, Mater. Chem. Phys. 248 (2020). doi:10.1016/j.matchemphys.2020.122908.

[7] P.J. Mafa, U.S. Swana, D. Liu, J. Gui, B.B. Mamba, A.T. Kuvarega, Synthesis of Bi5O7I-MoO3 photocatalyst via simultaneous calcination of BiOI and MoS2 for visible light degradation of ibuprofen, Colloids Surfaces A Physicochem. Eng. Asp. 612 (2021) 126004. doi:10.1016/j.colsurfa.2020.126004.

[8] S. Wu, H. Hu, Y. Lin, J. Zhang, Y.H. Hu, Visible light photocatalytic degradation of tetracycline over TiO2, Chem. Eng. J. 382 (2020) 122842. doi:10.1016/j.cej.2019.122842.

[9] A. V. Emeline, V. Ryabchuk, N. Serpone, Factors affecting the efficiency of a photocatalyzed process in aqueous metal-oxide dispersions Prospect of distinguishing between two kinetic models, J. Photochem. Photobiol. A Chem. 133 (2000) 89–97. doi:10.1016/S1010-6030(00)00225-2.

[10] M.M. Emara, S.H. Ali, A.A. Hassan, T.S.E. Kassem, P.G. Van Patten, How does photocatalytic activity depend on adsorption, composition, and other key factors in mixed metal oxide nanocomposites?, Colloids Interface Sci. Commun. 40 (2021) 100341. doi:10.1016/j.colcom.2020.100341.

[11] I.A. de Castro, R.S. Datta, J.Z. Ou, A. Castellanos-Gomez, S. Sriram, T. Daeneke, K. Kalantar-zadeh, A. Castellanos-Gomez, S. Sriram, T. Daeneke, K. Kalantar-zadeh,

Molybdenum Oxides – From Fundamentals to Functionality, Adv. Mater. 29 (2017) 1701619. doi:10.1002/adma.201701619.

[12] S. Adhikari, H.H. Lee, D.H. Kim, Efficient visible-light induced electron-transfer in z-scheme MoO3/Ag/C3N4 for excellent photocatalytic removal of antibiotics of both ofloxacin and tetracycline, Chem. Eng. J. 391 (2020) 123504. doi:10.1016/j.cej.2019.123504.

[13] J. Wang, X. Lei, C. Huang, L. Xue, W. Cheng, Q. Wu, Fabrication of a novel MoO3/Zn–Al LDHs composite photocatalyst for efficient degradation of tetracycline under visible light irradiation, J. Phys. Chem. Solids. 148 (2021) 109698. doi:10.1016/j.jpcs.2020.109698.

[14] G. Alnaggar, A. Hezam, Q.A. Drmosh, S. Ananda, Sunlight-driven activation of peroxymonosulfate by microwave synthesized ternary MoO3/Bi2O3/g-C3N4 heterostructures for boosting tetracycline hydrochloride degradation, Chemosphere. 272 (2021) 129807. doi:10.1016/j.chemosphere.2021.129807.

[15] S. Adhikari, H.H. Lee, D.-H. Kim, Efficient visible-light induced electron-transfer in z-scheme MoO3/Ag/C3N4 for excellent photocatalytic removal of antibiotics of both ofloxacin and tetracycline, Chem. Eng. J. 391 (2020) 123504. doi:10.1016/j.cej.2019.123504.

[16] D. Chen, Z. Xie, Y. Zeng, W. Lv, Q. Zhang, F. Wang, G. Liu, H. Liu, Accelerated photocatalytic degradation of quinolone antibiotics over Z-scheme MoO3/g-C3N4 heterostructure by peroxydisulfate under visible light irradiation: Mechanism; kinetic; and products, J. Taiwan Inst. Chem. Eng. 104 (2019) 250–259. doi:10.1016/j.jtice.2019.08.007.

[17] S. Sharma, S. Basu, Visible-light-driven efficient photocatalytic abatement of recalcitrant

pollutants by centimeter-length MoO3/SiO2 monoliths with long service life, Appl. Mater. Today. 23 (2021) 101033. doi:10.1016/j.apmt.2021.101033.

[18] F. Aoudjit, F. Touahra, L. Aoudjit, O. Cherifi, D. Halliche, Efficient solar heterogeneous photocatalytic degradation of metronidazole using heterojunction semiconductors hybrid nanocomposite, layered double hydroxides, Water Sci. Technol. 82 (2020) 2837–2846. doi:10.2166/wst.2020.519.

[19] M.E. Mahmoud, S.R. Saad, A.M. El-Ghanam, R.H.A. Mohamed, Developed magnetic Fe3O4–MoO3-AC nanocomposite for effective removal of ciprofloxacin from water, Mater. Chem. Phys. 257 (2021) 123454. doi:10.1016/j.matchemphys.2020.123454.

[20] J. Peña-Bahamonde, C. Wu, S.K. Fanourakis, S.M. Louie, J. Bao, D.F. Rodrigues, Oxidation state of Mo affects dissolution and visible-light photocatalytic activity of MoO3 nanostructures, J. Catal. 381 (2020) 508–519. doi:10.1016/j.jcat.2019.11.035.

[21] S.K. Misra, A. Dybowska, D. Berhanu, S.N. Luoma, E. Valsami-Jones, The complexity of nanoparticle dissolution and its importance in nanotoxicological studies, Sci. Total Environ. 438 (2012) 225–232. doi:10.1016/j.scitotenv.2012.08.066.

[22] Y. Liu, B. Zhang, Y. Yang, Z. Chang, Z. Wen, Y. Wu, Polypyrrole-coated α-MoO3 nanobelts with good electrochemical performance as anode materials for aqueous supercapacitors, J. Mater. Chem. A. 1 (2013) 13582–13587. doi:10.1039/c3ta12902k.

[23] V. Balakumar, H.H. Kim, R. Manivannan, H.H. Kim, J.W. Ryu, G. Heo, Y.A. Son, Ultrasound-assisted method to improve the structure of CeO2@polyprrole core-shell nanosphere and its photocatalytic reduction of hazardous Cr6+, Ultrason. Sonochem. 59 (2019) 104738. doi:10.1016/j.ultsonch.2019.104738.

[24] S. Sathiyanarayanan, S. Muthukrishnan, G. Venkatachari, D.C. Trivedi, Corrosion

protection of steel by polyaniline (PANI) pigmented paint coating, Prog. Org. Coatings. 53 (2005) 297–301. doi:10.1016/j.porgcoat.2005.03.007.

[25] W. Wang, J. Xu, L. Zhang, S. Sun, Bi2WO6/PANI: An efficient visible-light-induced photocatalytic composite, Catal. Today. 224 (2014) 147–153. doi:10.1016/j.cattod.2013.11.030.

[26] Y. Zhang, G. Zhao, Y. Jiang, W. Hong, Y. Zhang, M. Deng, H. Shuai, W. Xu, G. Zou, H. Hou, X. Ji, Monocrystal Cu3Mo2O9 confined in polyaniline protective layer: An effective strategy for promoting lithium storage stability, ChemElectroChem. 6 (2019) 1668–1695. doi:10.1002/celc.201801753.

[27] S.K. Fanourakis, S.Q. Barroga, J.V.D. Perez, L. He, D.F. Rodrigues, In Situ Polymerization of Polypyrrole and Polyaniline on the Surface of Magnetic Molybdenum Trioxide Nanoparticles: Implications for Water Treatment, ACS Appl. Nano Mater. 4 (2021) 12415–12428. doi:10.1021/acsanm.1c02873.

[28] A. Yadav, H. Kumar, R. Sharma, R. Kumari, Influence of polyaniline on the photocatalytic properties of metal nanocomposites: A review, Colloids Interface Sci. Commun. 40 (2021) 100339. doi:10.1016/j.colcom.2020.100339.

[29] J. Xu, Y. Hu, C. Zeng, Y. Zhang, H. Huang, Polypyrrole decorated BiOI nanosheets: Efficient photocatalytic activity for treating diverse contaminants and the critical role of bifunctional polypyrrole, J. Colloid Interface Sci. 505 (2017) 719–727. doi:10.1016/j.jcis.2017.06.054.

[30] M.M. Sundaram, M. Sangareswari, P. Muthirulan, Enhanced Photocatalytic Activity of Polypyrrole/TiO 2 Nanocomposites for Acid Violet Dye Degradation under UV Irradiation, IJIRSE) Int. J. Innov. Res. Sci. Eng. ISSN. (2014) 2347–3207.

[31] L. Zheng, Y. Xu, D. Jin, Y. Xie, Polyaniline-intercalated molybdenum oxide nanocomposites: Simultaneous synthesis and their enhanced application for supercapacitor, Chem. - An Asian J. 6 (2011) 1505–1514. doi:10.1002/asia.201000770.

[32] Y. Deng, L. Tang, G. Zeng, H. Dong, M. Yan, J. Wang, W. Hu, J. Wang, Y. Zhou, J. Tang, Enhanced visible light photocatalytic performance of polyaniline modified mesoporous single crystal TiO 2 microsphere, Appl. Surf. Sci. 387 (2016) 882–893. doi:10.1016/j.apsusc.2016.07.026.

[33] V. Gilja, K. Novaković, J. Travas-Sejdic, Z. Hrnjak-Murgić, M.K. Roković, M. Žic, Stability and synergistic effect of polyaniline/TiO2 photocatalysts in degradation of Azo dye in wastewater, Nanomaterials. 7 (2017). doi:10.3390/nano7120412.

[34] H.S. Kim, H.L. Hobbs, L. Wang, M.J. Rutten, C.C. Wamser, Biocompatible composites of polyaniline nanofibers and collagen, Synth. Met. 159 (2009) 1313–1318. doi:10.1016/j.synthmet.2009.02.036.

[35] U. Riaz, S.M. Ashraf, J. Kashyap, Enhancement of photocatalytic properties of transitional metal oxides using conducting polymers: A mini review, Mater. Res. Bull. 71 (2015) 75–90. doi:10.1016/j.materresbull.2015.06.035.

[36] N. Wang, J. Li, W. Lv, J. Feng, W. Yan, Synthesis of polyaniline/TiO2 composite with excellent adsorption performance on acid red G, RSC Adv. 5 (2015) 21132–21141. doi:10.1039/c4ra16910g.

[37] S. Dhanavel, E. Nivethaa, V. Narayanan, A. Stephen, Visible Light Induced Photocatalytic Degradation of Methylene Blue using Polyaniline Modified Molybdenum Trioxide, Mechanika. 9 (2017) 1–6. doi:10.2412/mmse.63.64.916.

[38] R. Saravanan, E. Sacari, F. Gracia, M.M. Khan, E. Mosquera, V.K. Gupta, Conducting

PANI stimulated ZnO system for visible light photocatalytic degradation of coloured dyes, J. Mol. Liq. 221 (2016) 1029–1033. doi:10.1016/j.molliq.2016.06.074.

[39] M. Ahmadi, H. Ramezani Motlagh, N. Jaafarzadeh, A. Mostoufi, R. Saeedi, G. Barzegar, S. Jorfi, Enhanced photocatalytic degradation of tetracycline and real pharmaceutical wastewater using MWCNT/TiO2 nano-composite, J. Environ. Manage. 186 (2017) 55–63. doi:10.1016/j.jenvman.2016.09.088.

[40] G. Herrera, J. Peña-Bahamonde, S. Paudel, D.F. Rodrigues, The role of nanomaterials and antibiotics in microbial resistance and environmental impact: an overview, Curr. Opin. Chem. Eng. 33 (2021). doi:10.1016/j.coche.2021.100707.

[41] R. Vasallo-Antonio, J. Peña-Bahamonde, M.D. Susman, F.C. Ballesteros, D.F. Rodrigues, Design and performance of Fe3O4@SiO2/MoO3/polydopamine-graphene oxide composites for visible light photocatalysis, Emergent Mater. (2021). doi:10.1007/s42247-020-00142-w.

[42] C. Liu, H. Tai, P. Zhang, Z. Yuan, X. Du, G. Xie, Y. Jiang, A high-performance flexible gas sensor based on self-assembled PANI-CeO2 nanocomposite thin film for trace-level NH3 detection at room temperature, Sensors Actuators, B Chem. 261 (2018) 587–597. doi:10.1016/j.snb.2017.12.022.

[43] A.A. Levinson, Analytical methods for atomic absorption spectrophotometry, Geochim. Cosmochim. Acta. 33 (1969) 1315–1316. doi:10.1016/0016-7037(69)90053-2.

[44] S.A. Glazier, J.J. Horvath, Feasibility of fluorescence detection of tetracycline in media mixtures employing a fiber optic probe, Anal. Lett. 28 (1995) 2607–2624. doi:10.1080/00032719508007413.

[45] U. Alam, S. Kumar, D. Bahnemann, J. Koch, C. Tegenkamp, M. Muneer, Harvesting visible

light with MoO3 nanorods modified by Fe(iii) nanoclusters for effective photocatalytic degradation of organic pollutants, Phys. Chem. Chem. Phys. 20 (2018) 4538–4545. doi:10.1039/c7cp08206a.

[46] B. Feng, Z. Wu, J. Liu, K. Zhu, Z. Li, X. Jin, Y. Hou, Q. Xi, M. Cong, P. Liu, Q. Gu, Combination of ultrafast dye-sensitized-assisted electron transfer process and novel Z-scheme system: AgBr nanoparticles interspersed MoO3 nanobelts for enhancing photocatalytic performance of RhB, Appl. Catal. B Environ. 206 (2017) 242–251. doi:10.1016/j.apcatb.2017.01.029.

[47] Z. Xie, Y. Feng, F. Wang, D. Chen, Q. Zhang, Y. Zeng, W. Lv, G. Liu, Construction of carbon dots modified MoO3/g-C3N4 Z-scheme photocatalyst with enhanced visible-light photocatalytic activity for the degradation of tetracycline, Appl. Catal. B Environ. 229 (2018) 96–104. doi:10.1016/j.apcatb.2018.02.011.

[48] L. Monser, F. Darghouth, Rapid liquid chromatographic method for simultaneous determination of tetracyclines antibiotics and 6-Epi-doxycycline in pharmaceutical products using porous graphitic carbon column, J. Pharm. Biomed. Anal. 23 (2000) 353–362. doi:10.1016/S0731-7085(00)00329-0.

[49] Y. Zhang, Z. Jiao, Y. Hu, S. Lv, H. Fan, Y. Zeng, J. Hu, M. Wang, Removal of tetracycline and oxytetracycline from water by magnetic Fe3O4@graphene, Environ. Sci. Pollut. Res. 24 (2017) 2987–2995. doi:10.1007/s11356-016-7964-7.

[50] J. Wu, Y. Jiang, L. Zha, Z. Ye, Z. Zhou, J. Ye, H. Zhou, Tetracycline degradation by ozonation, and evaluation of biodegradability and toxicity of ozonation byproducts, Can. J. Civ. Eng. 37 (2010) 1485–1491. doi:10.1139/L10-100.

[51] B.F. Spisso, A.L. de Oliveira e Jesus, M.A.G. de Araújo Júnior, M.A. Monteiro, Validation

of a high-performance liquid chromatographic method with fluorescence detection for the simultaneous determination of tetracyclines residues in bovine milk, Anal. Chim. Acta. 581 (2007) 108–117. doi:10.1016/j.aca.2006.08.004.

[52] E. Gill, A. Arshak, K. Arshak, O. Korostynska, pH sensitivity of novel PANI/PVB/PS3 composite films, Sensors. 7 (2007) 3329–3346. doi:10.3390/s7123329.

[53] I. Sapurina, J. Stejskal, The mechanism of the oxidative polymerization of aniline and the formation of supramolecular polyaniline structures, Polym. Int. 57 (2008) 1295–1325. doi:10.1002/pi.2476.

[54] R.D. Pyarasani, T. Jayaramudu, A. John, Polyaniline-based conducting hydrogels, J. Mater. Sci. 54 (2019) 974–996. doi:10.1007/s10853-018-2977-x.

[55] H. Li, S. Sun, H. Ji, W. Liu, Z. Shen, Enhanced activation of molecular oxygen and degradation of tetracycline over Cu-S4 atomic clusters, Appl. Catal. B Environ. 272 (2020) 118966. doi:10.1016/j.apcatb.2020.118966.

[56] A. Kumar, A Review on the Factors Affecting the Photocatalytic Degradation of Hazardous Materials, Mater. Sci. Eng. Int. J. (2017). doi:10.15406/mseij.2017.01.00018.

[57] H. Liu, J. Qu, T. Zhang, M. Ren, Z. Zhang, F. Cheng, D. He, Y. nan Zhang, Insights into degradation pathways and toxicity changes during electro-catalytic degradation of tetracycline hydrochloride, Environ. Pollut. 258 (2020) 113702. doi:10.1016/j.envpol.2019.113702.

[58] L. Yi, L. Zuo, C. Wei, H. Fu, X. Qu, S. Zheng, Z. Xu, Y. Guo, H. Li, D. Zhu, Enhanced adsorption of bisphenol A, tylosin, and tetracycline from aqueous solution to nitrogen-doped multiwall carbon nanotubes via cation-π and π-π electron-donor-acceptor (EDA) interactions, Sci. Total Environ. 719 (2020) 137389. doi:10.1016/j.scitotenv.2020.137389.

[59] S. Bai, Y. Zhao, J. Sun, Z. Tong, R. Luo, D. Li, A. Chen, Preparation of conducting films based on α-MoO3/PANI hybrids and their sensing properties to triethylamine at room temperature, Sensors Actuators B Chem. 239 (2017) 131–138. doi:10.1016/j.snb.2016.07.174.

[60] K.R. Anilkumar, A. Parveen, G.R. Badiger, M.V.N. Ambika Prasad, Effect of molybdenum trioxide (MoO3) on the electrical conductivity of polyaniline, Phys. B Condens. Matter. 404 (2009) 1664–1667. doi:10.1016/j.physb.2009.01.046.

[61] H. Ramezanalizadeh, E. Rafiee, Very fast photodegradation of tetracycline by a novel ternary nanocomposite as a visible light driven photocatalyst, Mater. Chem. Phys. 261 (2021). doi:10.1016/j.matchemphys.2021.124242.

[62] Z. Zhu, S. Wan, Q. Lu, Q. Zhong, Y. Zhao, Y. Bu, A highly efficient perovskite oxides composite as a functional catalyst for tetracycline degradation, Sep. Purif. Technol. 281 (2022). doi:10.1016/j.seppur.2021.119893.

[63] S. Wu, H. Hu, Y. Lin, J. Zhang, Y.H. Hu, Visible light photocatalytic degradation of tetracycline over TiO2, Chem. Eng. J. 382 (2020). doi:10.1016/j.cej.2019.122842.

[64] Y. Li, Y. Diao, X. Wang, X. Tian, Y. Hu, B. Zhang, D. Yang, Zn4B6O13: Efficient Borate Photocatalyst with Fast Carrier Separation for Photodegradation of Tetracycline, Inorg. Chem. 59 (2020) 13136–13143. doi:10.1021/acs.inorgchem.0c01425.

[65] J. Choina, A. Bagabas, C. Fischer, G.U. Flechsig, H. Kosslick, A. Alshammari, A. Schulz, The influence of the textural properties of ZnO nanoparticles on adsorption and photocatalytic remediation of water from pharmaceuticals, Catal. Today. 241 (2015) 47–54. doi:10.1016/j.cattod.2014.05.014.

[66] Y. Li, S. Wang, Y. Zhang, R. Han, W. Wei, Enhanced tetracycline adsorption onto

hydroxyapatite by Fe(III) incorporation, J. Mol. Liq. 247 (2017) 171–181. doi:10.1016/j.molliq.2017.09.110.

[67] Y. Zhao, X. Gu, S. Gao, J. Geng, X. Wang, Adsorption of tetracycline (TC) onto montmorillonite: Cations and humic acid effects, Geoderma. 183–184 (2012) 12–18. doi:10.1016/j.geoderma.2012.03.004.

[68] A.K. Das, S.K. Karan, B.B. Khatua, High energy density ternary composite electrode material based on polyaniline (PANI), molybdenum trioxide (MoO3) and graphene nanoplatelets (GNP) prepared by sono-chemical method and their synergistic contributions in superior supercapacitive performance, Electrochim. Acta. 180 (2015) 1–15. doi:10.1016/j.electacta.2015.08.029.

[69] M. Kumar Trivedi, Spectroscopic Characterization of Chloramphenicol and Tetracycline: An Impact of Biofield Treatment, Pharm. Anal. Acta. 06 (2015) 3–8. doi:10.4172/2153-2435.1000395.

[70] A. Bayu, D. Nandiyanto, R. Oktiani, R. Ragadhita, How to Read and Interpret FTIR Spectroscope of Organic Material, Indones. J. Sci. Technol. 4 (2019) 97–118.

[71] Y. Zhao, F. Tong, X. Gu, C. Gu, X. Wang, Y. Zhang, Insights into tetracycline adsorption onto goethite: Experiments and modeling, Sci. Total Environ. 470–471 (2014) 19–25. doi:10.1016/j.scitotenv.2013.09.059.

[72] M.E. Parolo, M.C. Savini, J.M. Vallés, M.T. Baschini, M.J. Avena, Tetracycline adsorption on montmorillonite: pH and ionic strength effects, Appl. Clay Sci. 40 (2008) 179–186. doi:10.1016/j.clay.2007.08.003.

[73] A.L.P.F. Caroni, C.R.M. de Lima, M.R. Pereira, J.L.C. Fonseca, Tetracycline adsorption on chitosan: A mechanistic description based on mass uptake and zeta potential measurements,

Colloids Surfaces B Biointerfaces. 100 (2012) 222–228. doi:10.1016/j.colsurfb.2012.05.024.

[74] S. Álvarez-Torrellas, A. Rodríguez, G. Ovejero, J. García, Comparative adsorption performance of ibuprofen and tetracycline from aqueous solution by carbonaceous materials, Chem. Eng. J. 283 (2016) 936–947. doi:10.1016/j.cej.2015.08.023.

[75] B.K. Vu, O. Snisarenko, H.S. Lee, E.W. Shin, Adsorption of tetracycline on La-impregnated MCM-41 materials, Environ. Technol. 31 (2010) 233–241. doi:10.1080/09593330903453210.

[76] H. Wang, B. Liao, T. Lu, Y. Ai, G. Liu, Enhanced visible-light photocatalytic degradation of tetracycline by a novel hollow BiOCl@CeO2 heterostructured microspheres: Structural characterization and reaction mechanism, J. Hazard. Mater. 385 (2020) 121552. doi:10.1016/j.jhazmat.2019.121552.

[77] Y. Nosaka, A.Y. Nosaka, Generation and Detection of Reactive Oxygen Species in Photocatalysis, Chem. Rev. 117 (2017) 11302–11336. doi:10.1021/acs.chemrev.7b00161.